Pursuit - The Journal of Undergraduate Research at the University of Tennessee

Volume 6 | Issue 1 Article 6

April 2015

A New H4/5 Ordinary Chondrite from North West Saudi Arabia, Al Jawf 001

Logan Combs
University of Tennessee, Knoxville, jross26@vols.utk.edu

Elizabeth A. Gass
University of Tennessee, Knoxville, egass@vols.utk.edu

Pursuit: The Journal of Undergraduate
Research at the University of Tennessee

trace.tennessee.edu/pursuit

PURSUIT

A New H4/5 Ordinary Chondrite from North West Saudi Arabia, Al Jawf 001

LOGAN COMBS
Advisors: Dr. Harry Y. McSween, Dr. Lawrence Taylor

This research involves the classification and description for the newly discovered ordinary chondrite breccia, Al Jawf 001. Compositional analyses of olivine, pyroxene, and kamacite in each of the major clasts and matrix of the breccia were taken in order to determine its compositional group (H, L, or LL). Percent mean deviations (PMD) of Fe in pyroxenes were calculated for every major clast and matrix, in order to determine the petrologic type of the meteorite. The thermal history was ascertained by pyroxene thermometry and the metallographic cooling rate. The above methods yielded that Al Jawf 001 is an H4/5 chondrite with a peak metamorphic temperature of 750 oC - 850 oC and a cooling rate of 0.1 - 1.0 oC per million years. The high peak metamorphic temperature and slow cooling rate suggest a two-stage cooling-rate history for the H chondrite parent body. Al Jawf 001 provides valuable insight into the history of the H chondrite and adds to the vast amount of information available on ordinary chondrites, increasing our knowledge of the early solar system.

1. Introduction

Ordinary chondritic meteorites are the most common chondrite group, with a vast majority (~88%) of the recovered chondritic meteorites being in this category (Dodd, 1981). They are distinguished from other chondrite groups through their bulk Mg/Si and (Ca, Al, Ti)/Si values (Dodd, 1981). Their compositions vary in terms of total iron (Fe) content and distribution of Fe between metals (Fe^0) and silicates (Fe^{2+}) (Hutchison, 2004). Ordinary chondrites fall into one of three compositional groups: H, L, or LL, based on the variation of Fe distribution. Varying degrees of thermal metamorphism are represented by petrologic types 3 (pristine) to 6 (completely equilibrated) with petrologic type 7 showing evidence for the onset of melting. The petrologic type of a meteorite has been correlated to the depth within the original parent body from which the meteorite formed, with types 6 and 7 located near the center and type 3 located on the outermost portion of the parent body (Dodd, 1981). As equilibration increases, the grain sizes also increase and the boundaries of chondrules become less distinguishable from the surrounding materials. Because of the correlation between petrologic type, parent body, and texture of the grains, the history of the meteorite can be interpreted.

The 3.16 kg Al Jawf 001 meteorite was found in the desert of the Al Jawf region of northwest Saudi Arabia in 2013. It is an H 4/5 ordinary chondrite breccia. The name follows guidelines established by the Meteoritical Society and has been officially approved (1/7/2014). These guidelines include geographical location of the find, who collected the meteorite, its mass, and, finally, the classification. In this study, the chemical, mineralogical, and textural properties of the newly discovered Al Jawf 001, an H4/5 meteorite, are described, as well as the interpretation of the thermal history of the meteorite.

2. Methods

Petrography of the polished thin-sections was performed with a petrographic microscope, and the thin-sections were observed in both reflected and transmitted light. Chemical analyses of the minerals were performed with a Cameca SX100 electron microprobe, with beam energy of 15 KeV, current of 20 nanoamps, and a spot- size of 1-5 microns. The counting time for each element was 20 seconds. Elemental X-ray maps of the thin-sections were produced for Al, Ca, Cr, Fe, Mg, Ni, P, S, Si, and Ti. These maps and the software ENVI were used to determine the modal mineral abundances of Al Jawf 001.

The Co wt.% in kamacite throughout the sample was plotted versus the mol. % fayalite in olivine (Fa#). Olivine and pyroxene grains were identified using back-scattered electron (BSE) images and energy-dispersive spectroscopy (EDS). At least 5 olivine grains and 5 pyroxene grains in each clast were examined. In total, 47 olivine and 42 pyroxene grains were analyzed. Points in the cores and rims of the grains were analyzed in order to assess their compositional homogeneities and ranges. Using the averaged data obtained from these analyses, the mol.% fayalite (Fa#) was plotted against the mol.% ferrosilite (Fs#) to identify each of the major clasts as from an H, L, or LL chondrite.

The cooling rates of the clasts, and the chondrite as a whole, were determined by using the method designed by Wood (1967), with revised cooling-rate curves calculated by Willis and Goldstein (1981). The shortest distance from the center of a taenite grain to the border between the exsolved taenite and host kamacite was measured. Analyses of the Ni content of the taenite grains were taken from the center point of the exsolved grains and plotted on the metallographic cooling-rate curves.

High-Ca pyroxene is nearly indistinguishable from olivine in BSE images. However, using the Ca and Mg X-ray maps along with EDS, orthopyroxenes and adjacent high-Ca pyroxenes

were identified. Once located, points on either side (~10) of the grain boundary between the two pyroxenes were analyzed. These analyses were plotted on a pyroxene quadrilateral to obtain the peak metamorphic temperatures using the two-pyroxene geothermometer of Lindsley (1983).

3. Classification

The three compositional groups of ordinary chondrites, H, L, and LL, are characterized by a decreasing abundance of native Fe metal and an increasing molar Fe/(Fe+Mg), that is Fe#, in silicates from H to LL (Dodd, 1981). The compositional group was determined using two different methods formulated by Brearly et al. (1998) and by Rubin (1990). The petrologic type was determined through textural relationships and the extent of pyroxene equilibration (Huss et al., 2006). Using these methods, Al Jawf 001 was classified as an H4/5 chondrite.

The variation of Fe# content between the compositional groups is exhibited in both the pyroxene and olivine grains of the meteorite (Brearley and Jones, 1998). Analyses of these grains within the meteorite yielded average values of Fa 19.4 % in olivine and Fs 17.9 % in pyroxene. Each of the major clasts has average compositions that fall within the H chondrite compositional field, except for clast C (which was interpreted to be an impact melt) (**Figure 1).** There are several other compositional differences that distinguish between the main clasts. The meteorite also contains 8.1 vol.% FeNi metal, corresponding to a high-Fe (H) classification. The Co-content of kamacite increases from H to LL, and there are fields of Co wt.% in kamacite and Fa in olivine that correspond to the three compositional groups (Rubin, 1990). Kamacite grains throughout the sample were analyzed to obtain an average Co of 0.5 wt.%. When plotted against Fa 19.4% in olivine, the meteorite fits within the H3.7 to H6 field (**Figure 2).** These lines of evidence all point to an H compositional classification.

The petrologic type of Al Jawf 001 is characterized by the extent of equilibration in the pyroxene of each clast studied, both inter- and intra-homogeneities. Pyroxene becomes completely equilibrated at petrologic type 5, so there is a distinct boundary in the PMD of ferrosilite in pyroxene between petrologic types 4 and 5. PMDs of 5-20 correspond to petrologic type 4, and PMDs below 5 correspond to petrologic type 5 (Huss et al., 2006). The PMD of ferrosilite in pyroxene were calculated for each of the major clasts and the matrix. Clasts B, E, and the matrix (M) are type 4 with PMDs of 12.1, 5.7, and 7.4, respectively. Clasts A, D, F, and G are type 5 with PMDs of 3.8, 2.0, 1.9, and 3.1, respectively. Al Jawf 001 is therefore classified as an H4/5 ordinary chondrite genomict breccia.

4. Textural Characteristics

4.1 Clastic Textures

This meteorite is a breccia composed of clasts and comminuted matrix. The major clasts of this meteorite vary texturally. The type 4 clast B contains an abundance of chondrules, with sharply defined edges (**Figure 3a**). This texture contrasts the type 5 clast D, in which the edges of the chondrules begin to merge with the surrounding groundmass (**Figure 3b**). The clasts of petrologic type 4 have a fine-grained texture compared to those of type 5. The grains of the type 5 clasts have been more extensively recrystallized, and thus, have larger grain sizes. There are also varying amounts of shock-melt in the clasts, with clast C being nearly completely composed of shock-melt. Clast C contains some relict grains of olivine, surrounded by an overgrowth of low-Ca pyroxene. In contrast to the rest of the sample, there are minor amounts of FeNi metal and troilite in this clast. Through the center of clast C, there is glassy mesostasis containing skeletal crystallites of feldspar. There are rims of high-Ca pyroxene where the

low-Ca pyroxene overgrowth is in contact with the glassy mesostasis an obvious effect of re-equilibration. (**Figure 3a**)

4.2 Chondrule Textures

The chondrules in Al Jawf 001 range in size from 0.2 to 0.6 mm with an array of different textural types. The most abundant textural type of chondrule present in this meteorite is the porphyritic olivine-pyroxene chondrule (**Figure 4**). Barred-olivine chondrules also make up a significant portion of the observed chondrules (**Figure 5**). The other types that are present are granular chondrules (**Figure 6**), cryptocrystalline chondrules, and radial pyroxene chondrules.

5. Modal Mineralogy and Mineral Compositions

5.1 Modal Abundances

Al Jawf 001 has a modal mineral abundance typical of H chondrites. The major phases in this meteorite are olivine, low-Ca pyroxene, feldspathic mesostasis, and FeNi metal. Other minor mineral phases include troilite, merrillite, apatite, and chromite. The modal abundances were determined by creating X-ray maps of the elements Al, Ca, Cr, Fe, Mg, Ni, P, S, Si, and Ti. Specific elemental maps were layered, and areas were marked where the mineralogy was confirmed with electron probe analyses. The ENVI program was then utilized to identify areas in the maps with similar intensity-profiles. This method gave modal abundances as area %, which was assumed to equate to volume % (**Figure 7**). This assumption was made on the basis that the thin section is a representative sample of the meteorite as a whole. The 8.1 vol.% of FeNi metal in the sample converts to 17.9 wt% of the sample, when the specific gravity of the mineral phases is taken into consideration. The abundance of FeNi metal within Al Jawf 001 corresponds to the average value of FeNi metal typical for H chondrites, ~18 wt% (Rubin et al., 2004).

5.2 Olivine

The compositions of the olivine grains within an H chondrite are within the range $Fa_{16\text{-}20}$ (Lindsley, 1983). Olivine grains in each clast were measured, and the average Fa composition for each clast was calculated. The averages for the clasts occur within the H chondrite range and are as follows: A = $Fa_{20.0;}$ B = $Fa_{19.2;}$ C = $Fa_{16.5;}$ D = $Fa_{19.8;}$ E = $Fa_{19.8;}$ F = $Fa_{19.8;}$ G = $Fa_{19.9;}$ and Mn = $Fa_{20.1}$. Although C is an impact melt clast, its olivine composition falls within the H chondrite range. Table 1 gives representative analyses of the olivine.

5.3 Pyroxene

The composition range of pyroxene grains within an H chondrite is $Fs_{14.5\text{-}18}$ (Lindsley, 1983). The calculated averages for each clast except C fall within or nearly within the H chondrite range and are as follows: A= $Fs_{18.0}$, B= $Fs_{16.3}$, C= $Fs_{20.6}$, D= $Fs_{17.6}$, E= $Fs_{16.6}$, F= $Fs_{17.8}$, G= $Fs_{17.8}$, M= $Fs_{18.9}$. The pyroxene grains occurring within clast C overgrow olivine and high-Ca pyroxene; thus, the composition plots outside the H chondrite range. Representative pyroxene analyses can be found in Table 2. Pyroxene thermometry was performed as well and is discussed later in the paper.

5.4 Iron-nickel metal

The FeNi metal phases, kamacite and taenite, were abundant throughout the samples. In ordinary chondrites, kamacite contains 5-10 wt.% Ni, whereas taenite contains, on average, 30-70 wt.% Ni. Typically, the Ni-rich phase, taenite, was exsolved from the less Ni-rich phase, kamacite (**Figure 8**), typical of intergrowths of these phases. Although various ratios of kamacite to taenite were noted, only those that could be used to determine the metallographic

cooling rate were measured. Representative analyses of iron-nickel metal grains can be found in Table 3.

Within clasts of petrologic type 5, the taenite had an Fe average content of 64.6 wt.%, with an average Ni content of 35.5 wt.%. The kamacite average Fe content was 90.0 wt.%, and the average Ni content was 9.5 wt.%. Within clasts of petrologic type 4, the taenite average Fe content was 66.0 wt.%, and the average Ni content was 31.5 wt.%. The kamacite average Fe content was 91.3 wt.%, and the average Ni content was 7.4 wt.%. The total average percent Fe and Ni within taenite for the sample was 65.3 wt.% and 33.5 wt.%, respectively. The total average percent Fe and Ni content for the kamacite within the sample was 90.7 wt.% and 8.4 wt.%, respectively, with the remaining 0.9 wt.% comprised of trace elements.

5.5 Feldspathic Mesostasis

The feldspar minerals within this chondrite occur in the glassy mesostasis. This feldspath-rich mesostasis occurs within all clasts, with varying degrees of abundance. It frequently contains skeletal crystals within some chondrules or the areas around the chondrules. The clast with the highest abundance of mesostasis was clast C. Excluding clast C, the abundance of feldspathic mesostasis was uniform throughout the sample. This feldspathic mesostasis makes up 16.5 % of the sample by volume, a large portion of the meteorite.

6. Peak Metamorphic Temperature

Chondrites undergo various thermal-metamorphic processes. The "onion-shell" thermal model describes a parent body that was initially internally heated by the decay of ^{26}Al (Blinova et al., 2007). The greatest degree of thermal metamorphism occurred at the center of the parent body, a metric which has been correlated to the composition of the altered minerals. If a chondrite contains more than one petrologic type, the current assemblage has not undergone temperatures above the range of the lowest petrologic type. Pyroxene is often used to determine the peak metamorphic temperature, but pyroxene equilibration is not complete until petrologic type 5 has been attained (Huss et al., 2006).

During our research, points on both sides of the high- and low-Ca pyroxenes were analyzed. Those points were plotted on the modified pyroxene quadrilateral derived from Lindsley's two-pyroxene geothermometer. The most equilibrated clasts had peak metamorphic temperatures between 750 and 850 ^{o}C (**Figure 9**).

7. Metallographic Cooling Rate

There are several methods for measuring the metallographic cooling rate, but the selected method was originally devised by Wood (1967) and later revised by Willis and Goldstein to account for 10 wt% Ni (Willis and Goldstein, 1981). Wood's method (1967) involves measuring the Ni content in kamacite and taenite and can only be used if the taenite is in solid solution within the kamacite, exsolution due to intersection with the kamacite-taenite solvus. Also, the taenite must not come into contact with the outside of the kamacite grain, so that contamination which may alter the Ni content of the taenite is avoided.

The metallographic cooling rates that were calculated for Al Jawf indicate two separate events with different cooling rates. The first cooling rate (**Figure 10**) indicates a slow cooling rate of 0.1 to 1 ^{o}C per million years while the second indicates an extremely fast-cooling rate. However, the metals yielding these measurements were present in shock-melt veins **(Figure 8)**, and would not have been associated with the primary cooling rate, that was calculated to be slower than the expected rate for H4/5 chondrites.

8. Discussion

The newly classified meteorite, Al Jawf 001, was found to be a typical H4/5 ordinary chondrite breccia. Its peak metamorphic temperature and cooling rate suggest an interesting history of the H-chondrite parent body. Al Jawf 001 has experienced both a high peak-metamorphic temperature and a very-slow cooling rate for a meteorite of petrologic type 4/5. This is similar to the chondrites studied by Niekerk and colleagues (2014). Our results suggest a two-stage cooling history. Shortly after reaching the peak-metamorphic temperature, the H chondrite parent body was impacted and broken apart. The pieces cooled quickly to <700 ^{o}C and were then re-accreted into a rubble-pile body, with subsequent cooling at a much slower rate (Van Niekerk et al., 2014). This presents an interesting petrogenesis, with room for further studies. More research is needed on meteorites with similar cooling rates and equilibration temperatures to obtain a stronger base of support for this hypothesis.

9. Summary

Olivine, pyroxene, FeNi metal, sulfide, and phosphate minerals dominate the newly described meteorite, Al Jawf 001. It is a genomict breccia with the clasts and matrix from the same compositional group (H), but different petrologic types (Biscoff et al., 2006). Using two polished thin-sections, seven clasts in this breccia were examined and denoted as A-G, while the matrix was denoted as M. The clasts range in size up to 4 cm. The outlines of chondrules blur into the groundmass as recrystallization increases, distinguishing clasts of petrologic type 4 from those of petrologic type 5 (Hutchison, 2004).

In order to classify Al Jawf 001, the compositions of olivine and low-Ca pyroxene were analyzed in each of the major clasts and in the matrix, as well as the Co wt.% in kamacite. Also the ratios of low-Ca pyroxene to adjacent high-Ca pyroxene grains were analyzed to obtain peak-metamorphic temperatures. Finally, taenites adjacent to kamacite grains were analyzed to estimate the cooling rate of 0.1-1 ^{0}C per million years, from 750-850 ^{0}C, considerably slower than typical for H4/5 chondrites. A secondary shock-event that resulted in melt veins was also recorded. These methods yielded a classification of H4/5 and also suggest a two-stage cooling process. The study of Al Jawf 001 provides insight into the formation and history of the H chondrite parent body. This study supports the idea that the parent body accreted and equilibrated, was disrupted and brecciated, then reaccreted and slowly cooled throughout the rest of its history. This hypothesis could give a window into early solar system processes such as the formation of planetesimals and in turn, larger planetary bodies such as the Earth.

References

Bischoff A., Scott E. R. D., Metzler K., and Goodrich C. A. 2006. Nature and origins of meteoritic breccias. In *Meteorites and Early Solar System II*, edited by Lauretta D. S. and McSween H. Y. Tuscon, Arizona: LPI Publishing. pp. 679-710.

Blinova A., Amelin Y., and Samson C. 2007. Constraints on the cooling history of the H-chondrite parent body from phosphate and chondrule Pb-isotopic dates from Estacado. *Meteoritics & Planetary Science*. 42: 1337–1350.

Brearley A.J. and Jones R.H. 1998. Chondritic meteorites. *Reviews in Mineralogy and Geochemistry*. 36(3):1-3.398.

Dodd R. T. 1981. *Meteorites, A petrologic-chemical synthesis,* New York, New York: Cambridge University Press. pp. 77-131.

Huss G. R., Rubin A. E., and Grossman J. N. 2006. Thermal metamorphism in chondrites. In *Meteorites and Early Solar System II*, edited by Lauretta D. S. and McSween H. Y. Tuscon, Arizona: LPI Publishing. pp. 567-586.

Hutchison R. 2004. *Meteorites: A petrologic, chemical, and isotopic synthesis*. Cambridge, UK: Cambridge University Press. pp. 128-141.

Lindsley, D. H. 1983. Pyroxene thermometry. *American Mineralogist*. 68: 477- 493.

Rubin A. E., Trigo-Rodriguez J. M., Kunihiro T., Kallemeyn G. W., and Wasson J. T. 2005. Carbon-rich chondritic clast PV1 from the Plainview H-chondrite regolith breccia: Formation from H3 chondrite material by possible cometary impact. *Geochimica et Cosmochimica Acta*. 69: 3419-3430.

Rubin A. E. 1990. Kamacite and olivine in ordinary chondrites: Intergroup and intragroup relationships. *Geochimica et Cosmochimica Acta*. 54:1217-1232.

Van Niekerk D., Scott E. R. D., and Taylor G. J. 2014. Constraints on the Thermal and Impact History of Ordinary Chondrites from Two-Pyroxene Equilibration Temperatures. LPSC abstract 2374.

Willis J. and Goldstein J. I. 1981. A revision of metallographic cooling rate curves for chondrites. Proceedings, 12th Lunar and Planetary Science Conference. pp. 1135–1143.

Wood J. A. 1967. Chondrites: Their metallic minerals, thermal histories, and parent planets. *Icarus*. 6:1-49.

Figures

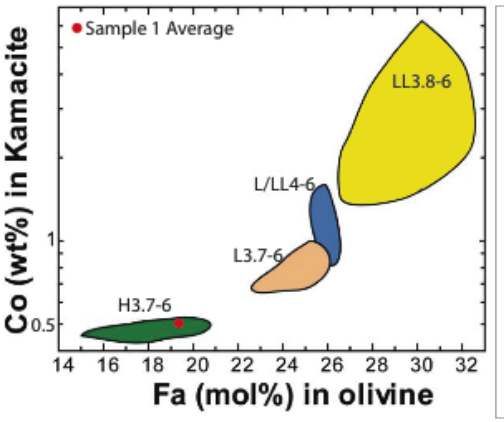

Figure 1: Average fayalite (Fa) and ferrosilite (Fs) compositions for each major clast and matrix plotted against each other for clasts in Al Jawf 001

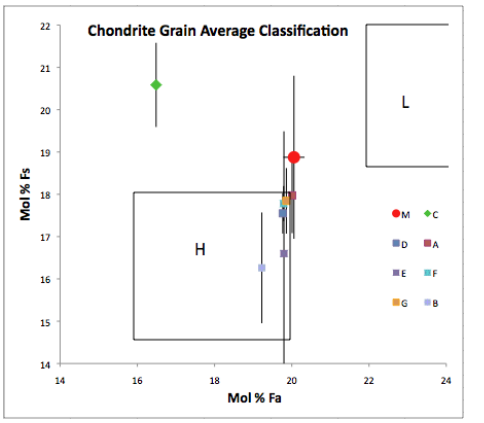

Figure 2: Weight percent of cobalt in kamacite vs the mol percent of fayalite in olivine found in Al Jawf 001

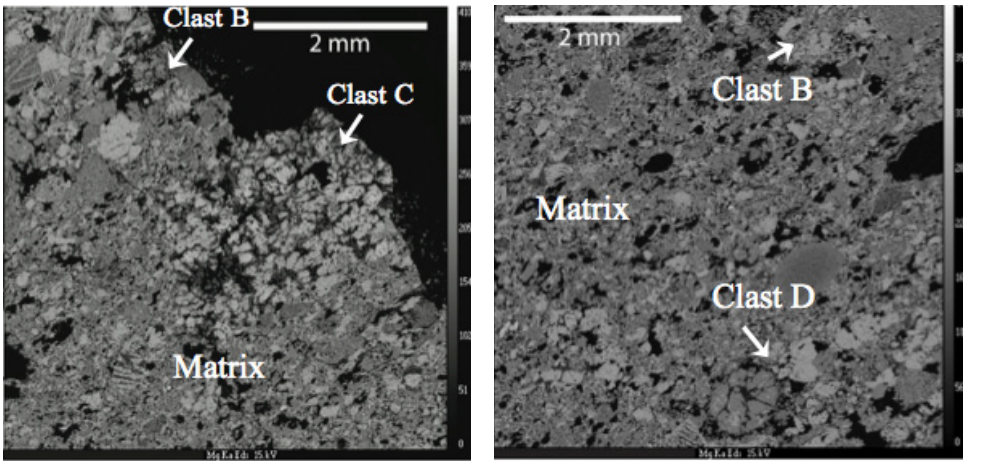

Figure 3: a) Magnesium X-ray map showing clast B (type 4) in the top left, clast C (impact melt) in the center, and the matrix (type 4) surrounding Clast C. b) Magnesium X-ray map showing Clast D (type 5) in the lower right, Clast B (type 4) in the top right and the matrix (type 4) in the center. Note the textural differences of the Clasts in Al Jawf 001.

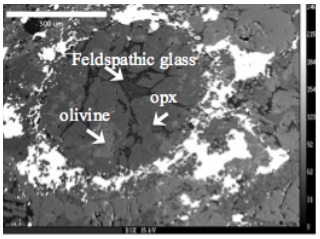

Figure 4: BSE image of a porphyritic chondrule in clast D surrounded by FeNi metal and troilite within the meteorite Al Jawf 001

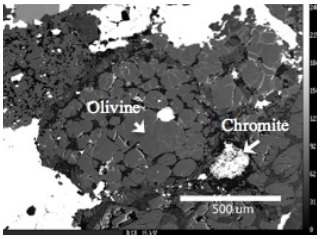

Figure 5: BSE image of a granular chondrule in clast D, within AL Jawf 001, with pyroxene along the edge.

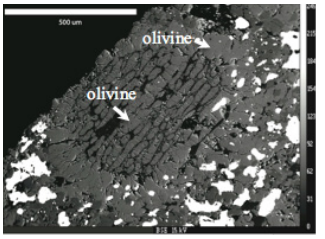

Figure 6: BSE image of a barred olivine chondrule in clast A enclosed by an olivine shell within the meteorite Al Jawf 001

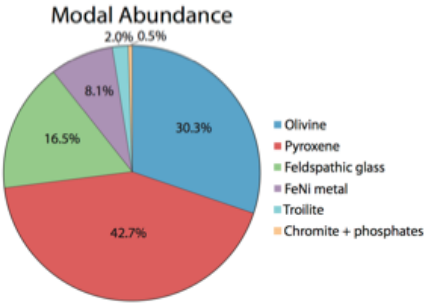

Figure 7: Modal abundance of Al Jawf 001. As derived from elemental x-ray maps.

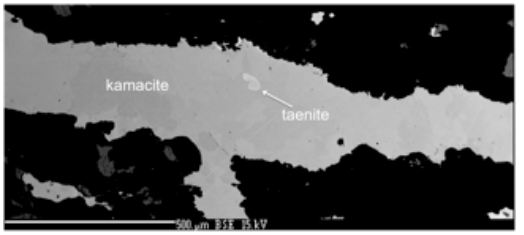

Figure 8: BSE image of a Kamacite metal vein containing exsolved taenite within Al Jawf 001. Light and dark areas within the kamacite result from variations in the nickel content.

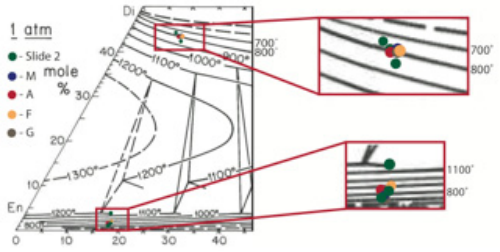

Figure 9: Modified pyroxene quadrilateral featuring isothermal contours, with our data that correspond to peak metamorphic temperatures determined from Ca content in adjacent high- and low-Ca pyroxenes found in Al Jawf 001

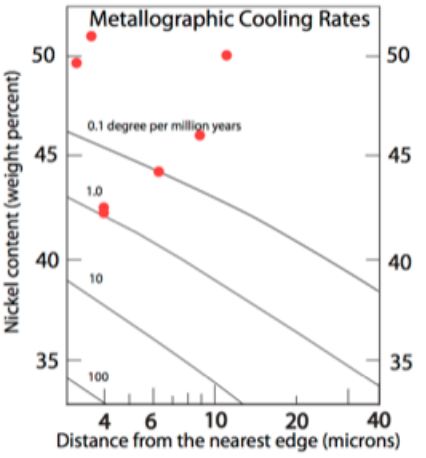

Figure 10: Metallographic cooling rate of Al Jawf 001. Weight percent of nickel in taenite plotted against distance, from the center of the taenite to the edge, on cooling rate curve with temperature in Kelvin. (Wood, 1967)

Representative Tables of Analyses

Table 1. Representative olivine analyses of the clasts in Al Jawf 001

	Clast A olivine-2	Clast B olivine-3	Clast C olivine-4	Clast D olivine-4	Clast E olivine-2	Clast F olivine-1	Clast G olivine-4	Matrix olivine-1
P_2O_5	0.03 (2)b	<0.03	<0.03	<0.03	0.12 (11)	0.04 (1)	<0.03	<0.03
SiO_2	39.2 (3)	39.1 (2)	39.0 (4)	39.1 (1)	39.0 (2)	39.1 (1)	38.9 (2)	39.0 (2)
TiO_2	<0.03	<0.03	<0.03	<0.03	<0.03	<0.03	<0.03	<0.03
Al_2O_3	<0.03	<0.03	<0.03	<0.03	<0.03	<0.03	<0.03	<0.03
Cr_2O_3	<0.03	<0.03	0.14 (4)	<0.03	<0.03	<0.03	<0.03	0.04 (1)
MgO	42.7 (3)	42.7 (2)	42.6 (10)	42.6 (3)	42.6 (3)	42.3 (2)	42.5 (2)	42.2 (3)
CaO	<0.03	<0.03	0.12 (2)	<0.03	0.03 (1)	0.05 (2)	<0.03	<0.03
MnO	0.45 (1)	0.47 (1)	0.43 (4)	0.45 (1)	0.45 (1)	0.47 (1)	0.46 (1)	0.46 (1)
FeO[a]	18.5 (2)	18.3 (4)	18.0 (13)	18.5 (1)	18.4 (2)	18.7 (2)	18.6 (1)	19.1 (1)
NiO	<0.03	<0.03	<0.03	<0.03	<0.03	<0.03	<0.03	<0.03
∑	100.88	100.48	100.29	100.65	100.6	100.56	100.46	100.8

Cations based on 4 oxygens

P	0.001	-	-	-	0.003	0.001	-	-
Si	0.993	0.992	0.992	0.991	0.989	0.994	0.99	0.991
Ti	-	-	-	0.001	-	-	-	-
Al	-	-	-	-	-	-	-	-
Cr	-	-	0.003	-	-	-	-	0.001
Mg	1.61	1.618	1.614	1.612	1.612	1.6	1.611	1.598
Ca	-	0.001	0.003	0.001	0.001	0.001	-	-
Mn	0.01	0.01	0.009	0.01	0.01	0.01	0.01	0.01
Fe2+	0.392	0.387	0.383	0.393	0.391	0.397	0.395	0.406
Ni	0.001	-	-	-	-	-	-	-
∑	3.007	3.009	3.004	3.008	3.006	3.003	3.006	3.006

[a] All Fe calculated as Fe^{2+}

[b] Units in ( ) represent one standard deviation in terms of least units cited

Table 2. Representative orthopyroxene measurements of the clasts in Al Jawf 001

	Clast A pyroxene-12	Clast B pyroxene-5	Clast C pyroxene-9	Clast D pyroxene-2	Clast E pyroxene-4	Clast F pyroxene-9	Clast G pyroxene-1	Matrix pyroxene-1
SiO_2	55.9 (6)[b]	56.1 (3)	55.1 (1)	56.3 (1)	56.4 (5)	56.3 (1)	56.4 (2)	56.4 (2)
TiO_2	0.19 (6)	0.19 (3)	0.08 (1)	0.08 (3)	0.08 (3)	0.17 (5)	0.05 (1)	0.09 (4)
Al_2O_3	0.18 (8)	0.22 (6)	0.41 (11)	0.15 (5)	0.07 (5)	0.16 (5)	0.04 (3)	0.16 (6)
Cr_2O_3	0.13 (6)	0.13 (4)	1.36 (14)	0.13 (4)	0.09 (3)	0.14 (3)	0.07 (1)	0.18 (7)
MgO	30.9 (4)	30.8 (2)	27.4 (5)	31.5 (1)	31.1 (2)	30.9 (1)	31.0 (2)	31.2 (2)
CaO	0.63 (9)	0.62 (4)	1.98 (24)	0.31 (8)	0.75 (2)	0.87 (10)	0.68 (18)	0.34 (10)
MnO	0.49 (1)	0.51 (2)	0.56 (3)	0.47 (2)	0.48 (1)	0.51 (2)	0.49 (3)	0.47 (3)
FeO[a]	12.4 (7)	11.41 (4)	13.3 (3)	11.6 (2)	11.8 (3)	11.8 (1)	11.9 (2)	11.9 (2)
Na_2O	---	---	0.06 (1)	---	---	---	---	---
∑	100.82	99.98	100.25	100.54	100.77	100.85	100.63	100.74

Cations based on 6 oxygens

Si	1.973	1.984	1.975	1.98	1.984	1.98	1.986	1.982
Ti	0.005	0.005	0.002	0.002	0.002	0.004	0.001	0.002
Al	0.008	0.009	0.017	0.007	0.003	0.007	0.002	0.007
Cr	0.004	0.004	0.038	0.003	0.003	0.004	0.002	0.005
Mg	1.623	1.627	1.468	1.653	1.63	1.619	1.63	1.637
Ca	0.024	0.024	0.076	0.012	0.028	0.033	0.025	0.013
Mn	0.015	0.015	0.017	0.014	0.04	0.015	0.015	0.014
Fe^{2+}	0.366	0.338	0.399	0.341	0.347	0.347	0.35	0.35
Na	0.001	0.001	0.004	-	0.001	0.001	0.001	0.001
∑	4.019	4.007	3.996	4.012	4.038	4.01	4.012	4.011

[a] All Fe calculated as Fe^{2+}

[b] Units in ( ) represent one standard deviation in terms of least units cited

Table 3. Representative kamacite and taenite analyses in wt% within Al Jawf 001

	Exsoved taenite-A1	Exsolved taenite-M4	Metal vein sample 2	Exsolved taenite-B1	M4 kamacite	A2 kamacite	E1 kamacite	Exsolved taenite-A3
Si	<0.03	<0.03	<0.03	<0.03	<0.03	<0.03	0.05	<0.03
S	<0.03	<0.03	<0.03	<0.03	<0.03	<0.03	<0.03	<0.03
Fe	49.1	49.1	92.5	55.2	93.9	89.2	93.1	49.1
Co	0.06	0.1	0.45	0.1	0.54	0.46	0.58	0.06
Ni	51.0	50.1	6.34	44.1	5.53	10.5	6.32	51.0
P	<0.03	<0.03	<0.03	<0.03	<0.03	<0.03	<0.03	<0.03
Mg	<0.03	<0.03	<0.03	<0.03	<0.03	<0.03	<0.03	<0.03
Al	0.17	<0.03	<0.03	<0.03	<0.03	<0.03	<0.03	0.17
Ti	<0.03	<0.03	<0.03	<0.03	<0.03	<0.03	<0.03	<0.03
Σ	100.33	99.3	99.29	99.4	99.97	100.16	100.05	100.33